

pubs.acs.org/EF Article

# Degradation Mechanism of Calcium Iridium Oxide for Oxygen Evolution Reaction in Acid

Published as part of Energy & Fuels virtual special issue "2023 Energy and Fuels Rising Stars". Ruihan Li, Jane Edgington, and Linsey Seitz\*



Cite This: Energy Fuels 2023, 37, 13554-13561



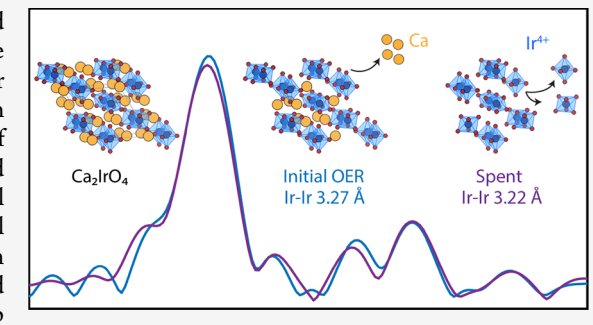
**ACCESS** 

III Metrics & More

Article Recommendations

SI Supporting Information

ABSTRACT: The development of active and acid-stable iridium-based catalysts is crucial to meet the requirements of proton exchange membrane technologies for the sustainable production of hydrogen via water electrolysis. However, long-term stability remains a critical challenge. In this work, we focus on a Ca<sub>2</sub>IrO<sub>4</sub> catalyst to develop a holistic picture of catalyst electronic and geometric structure evolution under various applied potentials by probing electrochemically active surface area, metal dissolution, Ir valence, and surface morphology. We observe an initial activity increase in parallel with increasing capacitance and minor iridium dissolution. Extensive chronoamperometry tests at oxidizing potentials lead to significant activity loss that occurs simultaneously with a dramatic drop in capacitance and a change in impedance. Using a combination of



electrochemical and spectroscopic tools, we provide fundamental insights to these material degradation processes to enable future catalyst design with balanced activity and long-term stability.

## INTRODUCTION

In pursuit of a sustainable energy landscape, electrocatalytic conversion processes, which enable the production of societally important fuels and chemicals, are envisioned to play an important role as we transition away from heavy reliance on fossil fuels. Water electrolysis is a promising technology to produce hydrogen via a carbon-free process. There is a critical need for active and acid-stable water splitting catalysts in order to meet the requirements of proton exchange membrane (PEM) electrolyzer technologies for the sustainable production of hydrogen. Iridium-based metal oxides are some of the most promising catalyst materials for the oxygen evolution reaction (OER) in acidic environments, given their relatively high activity and stability. Previous studies on nonstoichiometric iridium-based materials featuring  $A_{n+1}B_nO_{3n+1}$   $(n = 1 \text{ to } \infty)$ provide sufficient information regarding their short-term activity; however, long-term stability remains a critical challenge.2-5

Catalyst degradation can be driven by oxidation or dissolution in harsh acidic conditions, as well as other processes. The formation of nonconductive or semiconductive oxide layers, either from the reconstructed catalyst or support, isolates portions of the catalyst, prohibiting them from participating in the reaction. In addition, it has been reported that dissolution or transformation of Ir into other species is affected by potential, reaction current, surface composition, and the nature of the electrode. The authors found that metallic Ir can oxidize and dissolve as Ir<sup>3+</sup> or

transform to stabilized  ${\rm Ir}^{4+}$  or  ${\rm Ir}^{5+}$  species at moderately oxidizing potentials. At higher potentials (>1.6 V vs reversible hydrogen electrode, RHE),  ${\rm IrO}_3$  intermediates are formed, which can either dissolve in the form of  ${\rm IrO}_4^{2-}$  or redeposit on the catalyst surface. Overall, if transformation of iridium to other stable forms is favored over dissolution, this kinetic control will lead to a stable OER catalyst. Understanding the catalyst degradation or physicochemical changes that occur during continuous operation will help researchers mitigate these issues and inform design principles to balance catalyst activity and long-term stability.

Stability can be assessed by different electrochemical measurements, including variably or constant controlled potential, termed cyclic voltammetry (CV) or chronoamperometry (CA), respectively, or constant controlled current, termed chronopotentiometry (CP). Each protocol provides distinct insights into the system of interest. For CVs, catalysts are exposed to a constantly changing potential as they are repeatedly cycled, often in a wide potential window. This potential window may include potentials before OER current

Received: May 19, 2023 Revised: July 26, 2023 Published: August 15, 2023





onset, which can induce oxidation state or surface adsorbate coverage changes.<sup>12</sup> In contrast to this variable operation, CP and CA simulate a continuously operating device under constant current and voltage, respectively. Depending on the electrochemical protocol employed, it is possible for the reaction and degradation mechanisms to differ due to different modes of controlling the potential vs controlling the current.<sup>13</sup>

In much of the literature to date, catalyst stability is evaluated by conducting hundreds to thousands of CVs or long-term CPs at a single current density (i.e., 10 mA/cm<sup>2</sup> geo),3,5,14-21 but fundamental understanding of how materials respond to a wide range of oxidizing environments and their degradation mechanisms is lacking. During long-term CP tests, the potential may fluctuate in response to catalyst activity changes, induced by activation or degradation, in order to provide the set constant current. The fluctuating potentials may also trigger the restructuring of the catalyst surface or formation of new active site moieties. This uncontrolled potential fluctuation makes it difficult to study the catalyst's degradation mechanisms. In contrast, at a fixed potential, a catalyst experiences a constant overpotential or driving force for any reactions or surface restructuring. The current may increase if the catalyst surface transforms to a more active phase that is stabilized under reaction conditions or may decay over time due to the loss of active sites or increase in charge transfer resistance. Therefore, by conducting long-term CAs under various potentials, we are able to investigate the activity and stability of catalyst surface phases that are under constant operating conditions to gain insights to the associated reaction and degradation mechanisms.

Herein, we study the effect of oxidizing potentials on the catalytic performance of Ca<sub>2</sub>IrO<sub>4</sub> and material stability over long-term operation in acid. We employ stability protocols that alternate long, constant potential holds (CAs) with briefly cycled potentials (CVs) and electrochemical impedance spectroscopy (EIS) to induce material degradation primarily under a constant potential environment with periodic probes of the catalyst response and dynamic properties. We find that Ca<sub>2</sub>IrO<sub>4</sub> exhibits variable stability that is correlated with potential-dependent Ir dissolution pathways. EIS fitting and ex situ X-ray absorption spectroscopy (XAS) are employed to understand charge transport of the electrode and electronic structure of the catalyst material. Our results suggest that reconstructed surface phase with electrically insulating behavior forms during degradation, resulting in an inactive but stable surface that prevents further Ir dissolution after several hours of operation.

# ■ RESULTS AND DISCUSSION

**Pristine Material.** X-ray diffraction (XRD, Figure 1a) confirms the hexagonal crystal structure of  $Ca_2IrO_4$  reported in the literature. The minor peaks in the XRD pattern are attributed to CaO impurities. Since CaO is electrochemically inert, it does not contribute to the catalytic activity. High-resolution transmission electron microscopy (HRTEM, Figure 1b) shows the crystalline phase at the edge of pristine particle. The corresponding diffraction pattern matches well with the refined structure (space group  $P\overline{6}2m$ ) along the [011], [111], and [101] zone axes (Figure S1). Due to the high symmetry of the crystal structure, several zone axes can generate the same diffraction pattern. The micrometer-sized particles have a surface area of  $\sim$ 12 m²/g.

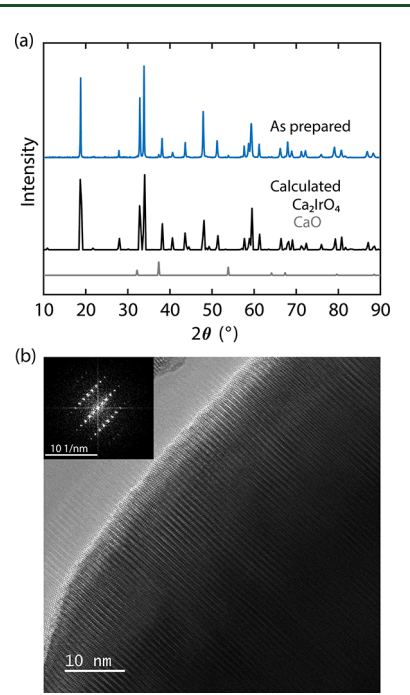


**Figure 1.** Characterization of the pristine material. (a) XRD of the asprepared powder. (b) HRTEM image along the [011] (or [111] or [101]) zone axis of  $Ca_2IrO_4$  with inset showing the fast Fourier transform.

## Effect of Oxidizing Potentials on Stability Outcomes.

To evaluate the activity evolution and long-term stability, Ca<sub>2</sub>IrO<sub>4</sub> catalyst powder was combined with an equal weight of Vulcan carbon support in an ink of 97% v/v isopropyl alcohol and 3% v/v Nafion 117 for deposition onto glassy carbon disk substrates. Extensive CAs at various oxidizing potentials, ranging from 1.65 to 1.576 V vs RHE, were applied to the electrodes in 0.1 M HClO<sub>4</sub> over 2-12 h, ensuring that these measurements would probe both activation and deactivation processes of the catalyst. CVs and impedance spectra were also recorded intermittently to monitor the activity, capacitance, and charge transfer resistance. At 1.60 V vs RHE, the electrode experiences three stages of activity evolution before completely losing its activity after 6 h testing (Figure 2). During the initial OER testing phase, designated with the label "0.25 h" in Figure 2, the activity increases in parallel with increasing capacitance. After this phase, the electrode enters a second, stable phase (as determined by intrinsic activity normalized to catalyst surface area, Figure 2c) for at least 2 h, before finally entering a third phase of slow degradation over more than 4 h. The electrode also exhibits a change in capacitance that correlates with OER activity evolution. While capacitance is broadly used in the literature to reflect changes in catalyst surface area and significant surface rearrangement, 3,5,20,23 we note that capacitance is also likely to vary with material intrinsic properties such as surface structure, composition, and conductivity. In this work, capacitance is used to estimate the change in electrochemically accessible catalyst surface area, while we also acknowledge possible changes in catalyst conductivity over the course of electrochemical testing, as monitored via EIS. 24,25 It is also likely that oxidation of the Vulcan carbon support or glassy carbon substrate obstructs the conductive path between the catalyst and the electrode contact, leading to a decrease in accessible sites over testing time. 25,26 During the degradation phase, which occurs during

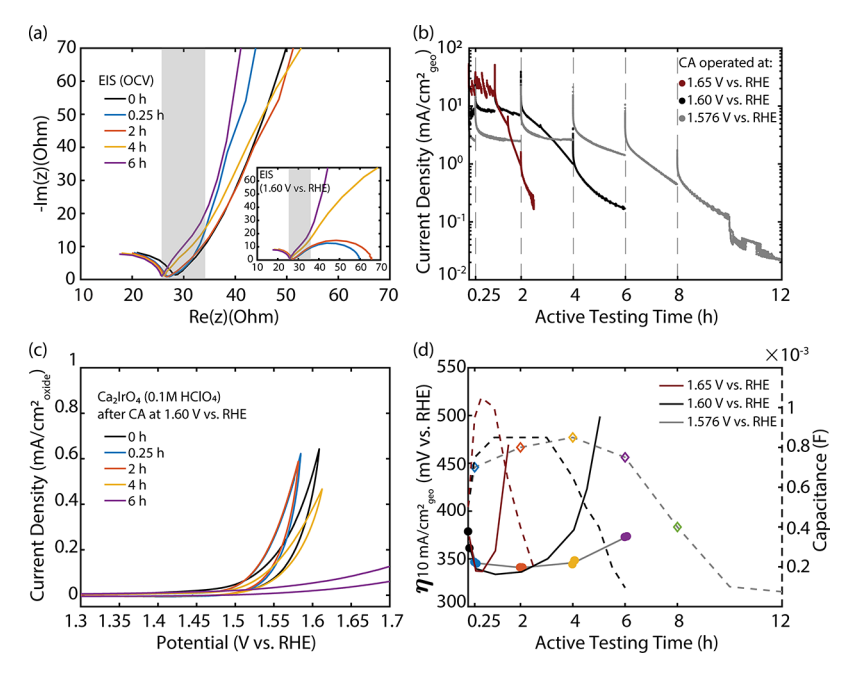


Figure 2. Electrochemical activity and stability of  $Ca_2IrO_4$  / glassy carbon electrodes. (a) EIS collected at OCV (inset: 1.60 V vs RHE) at several time points during a 6 h CA at 1.60 V vs RHE. The middle frequency regime where the arc is observed is marked in gray. (b) CAs showing current normalized by geometric area at various potentials. (c) CVs showing intrinsic current density at several time points during 6 h of electrochemical stability testing (1.60 V vs RHE, 0.1 M HClO<sub>4</sub>). (d) Evolution of overpotential (solid lines) required to reach 10 mA/cm<sup>2</sup><sub>geo</sub> and capacitance (dashed lines) as a function of active testing time during extensive CA at 1.65, 1.60, and 1.576 V vs RHE.

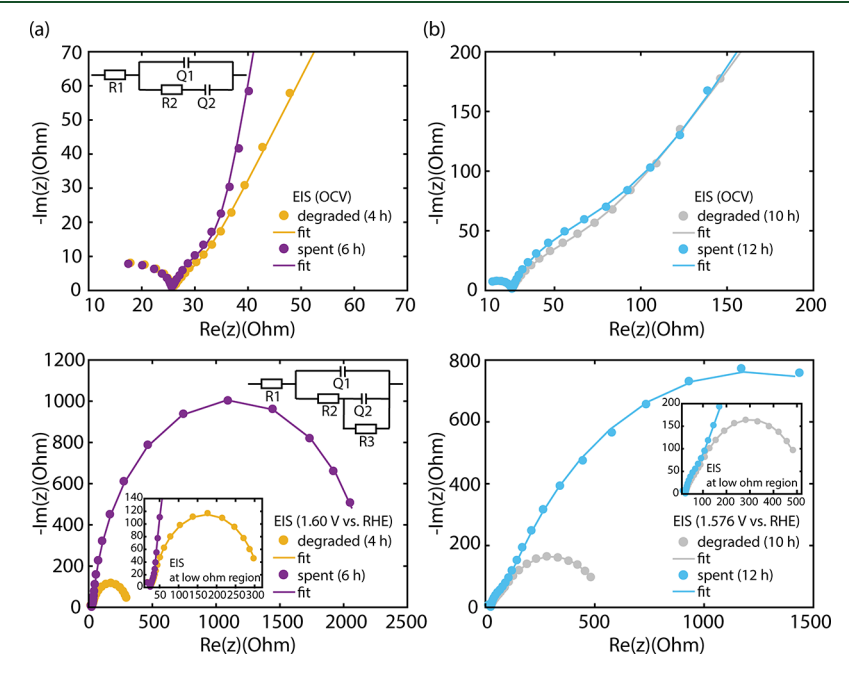


Figure 3. "Degraded" and "spent" impedance spectra (data points and fits) collected at OCV and oxidizing potentials during stability test operated at (a) 1.60 V vs RHE and (b) 1.576 V vs RHE. Inset figures include the data and fits at low impedance region, as well as equivalent circuits used for fitting.

the 4 and 6 h CAs (Figure 2), there is significant activity loss that occurs simultaneously with a large drop in capacitance and changes in conductivity, as revealed by impedance spectra. These activity, capacitance, and conductivity trends are similar for all electrodes prepared with Ca<sub>2</sub>IrO<sub>4</sub>, even when tested under different oxidizing potentials; however, the timescales for each of these stages differ (Figure 2b,d). Specifically, at 1.576 V vs RHE, the electrode performance begins to degrade most significantly after 6 h compared to degradation occurring

after 4 h or shorter at higher oxidizing potentials. Similarly, activity is considered completely lost after 12 h CA for the sample held at 1.576 V vs RHE compared to after 6 or 2 h when held at 1.60 and 1.65 V vs RHE, respectively.

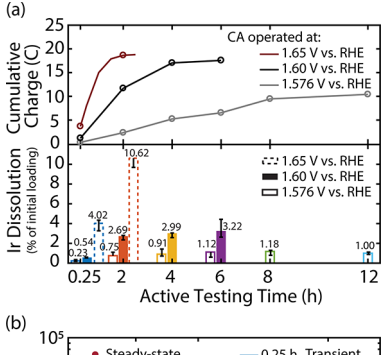
EIS is also used to investigate the electric properties of the electrode, including the substrate, catalyst, and catalyst interfaces with the substrate and electrolyte during degradation. Impedance spectra of the degraded and spent samples (at open circuit voltage (OCV)) reveal an arc in the middle-

frequency range (16000-150 Hz), which deviates from behavior of a Warburg element as used in typical Randles circuits (Figure 2a). Upon further investigation of EIS measured at the same potential as the respective CA holds for each sample, this arc is still present in the middle frequency regime for degraded and spent samples. To better understand the electrode properties that contribute to the features in the spectra, two equivalent circuits are used to fit the spectra collected during degradation (Figure 3). To fit the data under OCV, a modified Randles circuit was used; this circuit is composed of a resistor (R1, solution resistance) and a constant phase element (Q1), which is in parallel with a combination of a second resistor (R2) and a second constant phase element (Q2, in place of the Warburg element for a typical Randles circuit). To fit data at applied potentials, another resistor (R3) is added in parallel with the constant phase element (Q2). The arc in the middle-frequency range reflects behavior of the R2 resistor, which represents impediments to electron transfer between the electrolyte and electrode. Both fits of the impedance spectra collected under OCV and applied oxidizing potentials show a relatively constant value of the R2 resistor, suggesting that it is not caused by an electrochemical process, but a diffusive process (Tables S1 and S2). The impedance representation at low frequency reveals reaction kinetics;<sup>27</sup> specifically, the depressed semicircle feature present in the spectra measured under oxidizing potentials reflects the OER charge transfer kinetics, which is related to the parallel circuit of the Q2 constant phase element and R3 resistor. At 1.60 V vs RHE, the OER charge transfer resistance changes slightly during the 0.25-2 h testing time (inset, Figure 2a), consistent with the observation that the catalyst activity remains stable during this period. After 4 h of continuous testing at 1.60 V vs RHE, the increasing R3 resistance indicates increased charge transfer resistance for OER, which correlates with an observed decrease in activity. Furthermore, we calculate an increasing pseudo capacitance (C2), from the fitted Q2 constant phase element during degradation. This can be caused by several factors, such as inhomogeneity of the surface, variability in conductivity, grain boundaries, and crystal phases of polycrystalline electrode, which contribute to the distributed time constants of the constant phase element representation.<sup>28-30</sup> Overall, diffusive resistance is introduced and OER kinetics are impeded during degradation, correlating to an increase in the electrically insulating nature of the electrode.

Stability of Substrate. Electrode deactivation can be caused by degradation of the catalyst material itself as well as oxidation of the carbon substrate. 26,31 To determine the primary cause of our electrode deactivation and identify the contributions from both the glassy carbon substrate degradation and catalyst material degradation, a comparative study was conducted by oxidizing a bare glassy carbon disk at 1.65 V for 2 h, 1.60 V for 6 h, and 1.576 V for 12 h. These bare substrate oxidation treatments reflect the duration of electrode performance at each of these respective potentials, as presented in Figure 2. The impedance spectra (at OCV) for the oxidized bare glassy carbon disks show an increased diffusive resistance compared to the pristine disks (Figure S2a). However, the characteristic arc in the middle frequency regime disappears when Ca<sub>2</sub>IrO<sub>4</sub> catalyst ink is drop-cast on these preoxidized disks (Figure S2a-c). Furthermore, the initial activity and capacitance of the electrodes with catalyst are similar regardless of using pristine or preoxidized substrates, indicating that the impact of substrate oxidation is not strong enough to affect the

initial OER kinetics (Figure S2d). We also investigated the contribution of glassy carbon disk oxidation to the electrode degradation during long-term operation using the same electrochemical protocol for electrodes using glassy carbon disks that have been preoxidized at 1.60 V vs RHE for 6 h before drop-casting the ink on the disk surface. Again, the characteristic arc in the middle frequency regime appears only after the electrode degrades. The same evolution of impedance and activity, regardless of the status of substrate, suggests that this catalyst material degrades on a much faster scale than carbon oxidation (Figure S3). <sup>26</sup>

Stability of Surface Iridium. Many previous studies on Irbased materials have shown a correlation between OER activity and Ir dissolution in acid. Therefore, to determine the relationship between long-term electrode performance and metal dissolution from Ca<sub>2</sub>IrO<sub>4</sub>, we used inductively coupled plasma mass spectrometry (ICP-MS) to monitor iridium dissolution while holding identical electrodes at 1.576, 1.60, and 1.65 V vs RHE, until each electrode has completely lost activity. Figure 4 shows the cumulative OER



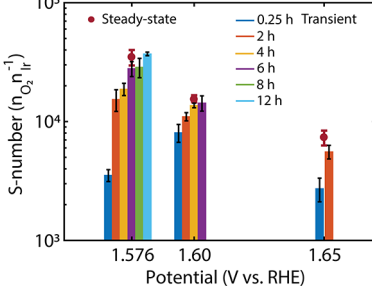


**Figure 4.** (a) Cumulative OER charge and Ir dissolution evolution (% of  $80~\mu \rm g_{Ir}/cm^2$ ) as a function of active testing time during extensive CA at varied potentials. Error bars show the deviation of three independent measurements. (b) S-numbers calculated from cumulative OER charge and Ir dissolved. Error bars show the standard deviation of three independent measurements.

charge passed for each of these electrodes and the Ir dissolution at each corresponding time point. Overall, we find that iridium leaching does not increase monotonically with charge. Electrodes tested at the two higher oxidizing potentials reach a maximum cumulative OER charge of approximately 20 C, after which point the electrodes lose nearly all activity. The electrode tested at the lowest potential only reaches a maximum cumulative OER charge of approximately 10 C. Ir dissolution from the electrodes ranges from 0.23 to 10.6% of the total Ir, with the highest Ir dissolution occurring upon exposure to the highest oxidizing potential (1.65 V vs RHE, Figure 4a). The electrode tested at 1.65 V vs RHE loses 10.6% of its total Ir loading to the electrolyte after only 2 h. In

contrast, the electrode tested at 1.60 V vs RHE experiences dissolution of 2.7% of its initial Ir loading in the first 2 h, followed by a period of relative stability where only an additional 0.5% of initial Ir loading is dissolved in the next 4 h, for a total of 3.2% Ir dissolved after 6 h of testing. Finally, the electrode tested at 1.576 V vs RHE experiences the least dissolution reaching nearly 1% dissolution after 4 h and maintaining close to this value for the remainder of the 12 h stability test. Furthermore, instead of simply comparing dissolution vs time, we can compare the amount of Ir dissolved vs OER charge passed for electrodes operated at different potentials. For example, we see that the same amount of OER charge has been passed for the electrode operated at 1.65 V vs RHE for 2 h (Figure 4a) and the electrode operated at 1.60 V vs RHE for 4 h (Figure 4a). Even though each sample has supported approximately the same number of reaction turnovers, the sample operated at higher potential has lost ~3.5× more Ir via dissolution. Together, these results indicate potential-dependent iridium dissolution pathways. We hypothesize that the lower potentials may support formation of surface Ir species that have slower dissolution kinetics and instead favor transformation to more stable Ir moieties.

As these electrodes generally experience higher rates of Ir dissolution during the initial testing period, it is likely that the catalyst surface is restructuring and exposing more surface area that leads to improved OER activity. After this initial period, the catalyst activity sharply declines (after 4 and 6 h at 1.60 and 1.576 V vs RHE, respectively), but iridium dissolution becomes negligible during this testing period as well. We note that the ICP measurements exclude any mechanical instability that may contribute to activity loss, as larger pieces of catalyst separating from the electrode are not detected. As mentioned in the previous section, the impact of substrate oxidation on electrode degradation is minimal and the electrode instability comes from the materials themselves. It is likely that a stable phase with increased insulating behavior forms, resulting in loss of activity during this testing period. Dissolution of active sites can also worsen the contact between catalyst and substrate. The different surface geometries formed under the reaction conditions affect the stability of surface atoms and dissolved species. Similar to what has been reported on RuO<sub>2</sub>, where surface geometry varies with potential, 32 varying extents of Ir leaching may leave behind different defective surfaces that affect the electron transport and OER performance.

As we further consider the relationship between Ir dissolution and OER charge passed, we evaluate the S-number for these electrodes. The S-number has been used as a metric to assess the stability of precious metal catalysts and it is defined as the ratio between the amount of evolved oxygen (calculated from OER charge) and the amount of dissolved iridium (extracted from ICP-MS data).<sup>33</sup> The higher the number, the more stable the active center of the electrocatalyst. Here, we used two methods of evaluating S-numbers to compare the stability of catalyst phases that are formed at different stages of stability testing (Figure 4b).<sup>34</sup> The "steadystate" S-number is calculated by generating a linear trendline using the total OER charge passed and amount of Ir dissolved, such that it represents behavior of the system once it has reached a steady state under reaction conditions. In contrast, the "transient" S-number is calculated based on the cumulative charge and the amount of dissolved Ir at each individual time point such that it reflects dynamic behavior of the catalyst material, especially highlighting changes during early stages of

stability testing. Both methods reveal a higher S-number at lower operating potentials. However, considering the transient S-number, we note that the S-numbers increase significantly with increased testing time, indicating that there are fast material dynamics occurring upon the first exposure to acid. Overall, we note that the sample operated at 1.60 V vs RHE may achieve the best compromise of performance and dissolution; it supported almost two-times greater OER charge compared to samples operated at 1.576 V and achieved higher steady-state (and transient) S-numbers compared to operation at 1.65 V vs RHE. Considering the S-number as a function of time, the reconstructed surface formed after initial OER at 1.60 V vs RHE is the most stable compared to surfaces formed on electrodes tested at other potentials. The S-number changes dramatically after 2 h CA at 1.576 V vs RHE, indicating a transformation to an active and stable phase. For each operating potential, degraded samples and spent samples show similar Ir dissolution and transient S-number, indicating the eventual stabilization of a reconstructed surface phase during degradation. It is possible that the formation of a thin, porous iridium oxide layer at the surface of a catalyst particle acts as an anchor to avoid further metal dissolution. Considering that the calculation of the S-number varies with electrochemical testing conditions employed, such as potentiostatic vs potentiodynamic measurements, operating time and potential, and calculation methods used (dynamic vs steadystate),<sup>34</sup> it is critical to compare S-numbers for materials that are tested under relevant reaction conditions to provide a more meaningful comparison of stability. The transient S-number of Ca<sub>2</sub>IrO<sub>4</sub> falls into a similar range with other iridates, such as  $Y_2Ir_2O_7^{35}$  and  $Ba_2PrIrO_6^{33}$  that were tested under a constant voltage at 1.60 V vs RHE for 2.5 h and 30 min, respectively. However, the steady-state S-numbers for Ca<sub>2</sub>IrO<sub>4</sub> calculated at 1.576 and 1.60 V vs RHE (45,250 and 15,376, respectively) are an order of magnitude lower than that of  $IrO_2^{36}$  (6.1 × 10<sup>5</sup>) and  $IrO_r^{33}$  (1 × 10<sup>5</sup>), indicating that the newly reconstructed surface formed under these testing conditions is less stable compared to pure iridium oxides.

Materials Characterization. To complement the electrochemical analysis and understand how materials respond to different reaction conditions, we employed several characterization techniques. Scanning electron microscopy/energy dispersive spectroscopy (SEM/EDS) was used to probe the distribution of elements before and after electrochemical testing, revealing that all metal elements are present in the bulk, even after extended testing and complete activity loss (Figure 5a). Similarly, X-ray diffractograms of electrodes after electrochemical testing display all the characteristic peaks for the hexagonal structure, confirming retention of bulk material crystallinity (Figure 5b).

Oxidation states and chemical species of surface Ir were assessed using X-ray photoelectron spectroscopy (XPS) for Ca<sub>2</sub>IrO<sub>4</sub> samples before and after 0.25, 2, 4, and 6 h of electrochemical OER testing (Figure 5c). The Ir 4f peaks are fit with two doublets (Ir 4f 7/2, Ir 4f 5/2) for all samples, with each doublet having a splitting of 1 eV, the same FWHM, and a relative area ratio of 4:3. The pristine sample is fitted with additional satellite peaks to achieve a good fitting (Table S3). Compared to pristine samples, both doublets shift to higher energy after electrochemical testing. After exposure to OER conditions, the Ir 4f peaks do not display a decrease in Ir signal or significant changes in position, shape, or area as a function of CA testing time. Ca 2p peaks reveal almost complete loss of

Energy & Fuels pubs.acs.org/EF Article

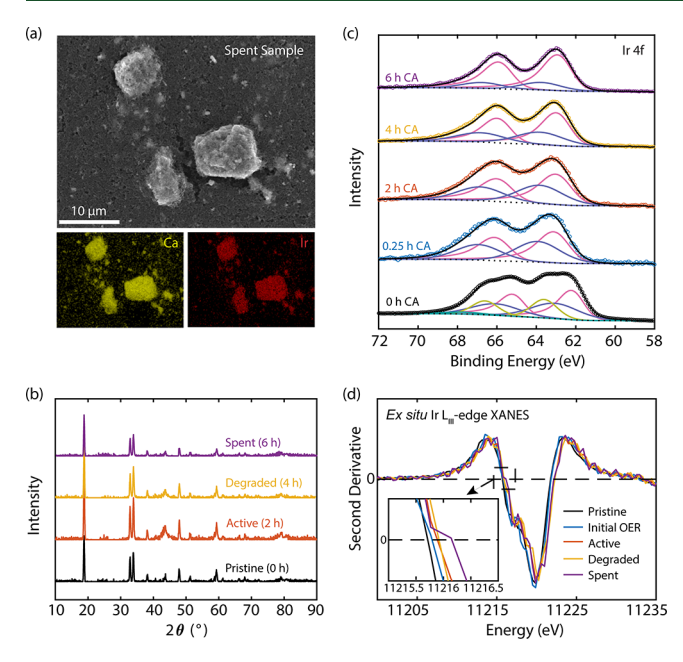


**Figure 5.** Ex situ characterization after electrochemical testing. (a) SEM/EDS images of the spent sample. (b) Shallow angle XRD showing bulk crystallinity. (c) Ir 4f XPS spectra after denoted time of CA. (d) Ir  $L_{\rm III}$ -edge XANES (second derivative) showing irreversible change in average, bulk Ir oxidation state after extensive CA at 1.60 V vs RHE.

intensity after 0.25 h of testing (Figure S5), indicating severe calcium leaching from the surface. Therefore, the constant Ir valence suggests a surface reconstruction that may maintain Ir of the 4+ state with possible surface reconstruction or amorphization. Alternatively, the stable Ir oxidation state may be a result of *ex situ* measurement conditions, where surface Ir returns to a 4+ state after removing the catalyst from reaction conditions, possibly due to high surface energies.

Bulk sensitive ex situ X-ray absorption near edge structure (XANES) at the Ir-L<sub>III</sub> edge was used to track changes in the average Ir oxidation state after exposing samples to various electrochemical conditions. Figure 5d shows the second derivative of spectra (Figure S6) averaged from seven separate measurements of each sample and condition, with an edge position uncertainty of ~0.19 eV for this data set (calculation details for uncertainty included in methods). The Ir edge position (second derivative zero crossing) increases slightly (~0.43 eV) after longer exposure to oxidizing potentials, indicating increased average Ir oxidation state. We hypothesize that the energy level of Ir 2p orbital in the new materials phase (surface reconstructed iridium oxide phase and bulk Ca<sub>2</sub>IrO<sub>4</sub>) increases after electrochemical testing. Long-time CA may increase the thickness of the reconstructed iridium oxide phase, overall, generating a larger percentage of this phase in the tested materials. The observed shifts between the pristine and the initial OER samples, as well as the shift between the degraded and the spent samples are beyond the uncertainty value of these measurements (0.19 eV), indicating clear trends as a function of increased testing time.

Ex situ extended X-ray absorption fine structure (EXAFS) and Fourier transform analysis were carried out to further investigate the geometric structure of iridium (Figure 6, Figure S7, Table S4). The negligible change in the Ir–O bond (1.99 Å) and coordination number ( $\sim$ 6) in the first shell throughout all samples indicates stable bulk [IrO<sub>6</sub>] octahedra during OER.

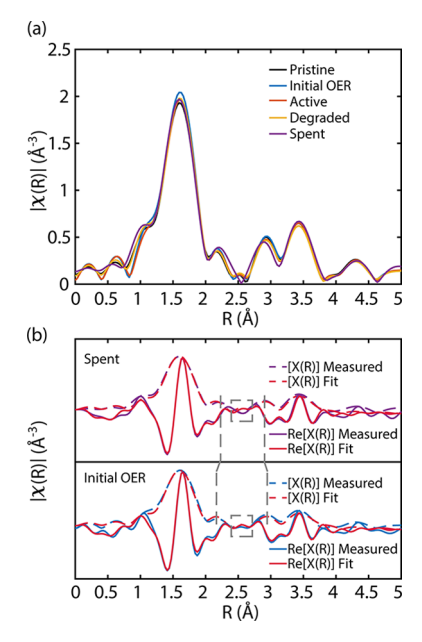


**Figure 6.** Ex situ EXAFS. (a) R space of all samples (pristine sample was measured in transmission mode, while the rest of the samples were measured in fluorescence mode). (b) EXAFS fitting of initial and spent samples (fitted R ranges from 1.1 to 3.9 Å, dashed lines showing the difference between two samples).

EXAFS fits (Table S4) of the pristine Ca<sub>2</sub>IrO<sub>4</sub> sample and rutile IrO<sub>2</sub> show a longer Ir-Ir bond in Ca<sub>2</sub>IrO<sub>4</sub> (3.27 Å) compared with that of edge-sharing octahedra of rutile IrO<sub>2</sub> (3.14 Å), indicating that the Ir-Ir bond is stretched due to additional bonding of Ir with Ca to match the expanded unit cell (Figure S1a). The spent sample spectrum differs most from the other spectra in the region of 2.0-3.2 Å of R space, where the peaks centered at ~2.1 and ~2.9 Å slightly shift (marked in dashed lines in Figure 6b), and the peak near 2.5 Å disappears (marked in rectangle in Figure 6b). EXAFS fits of initial and spent samples show that these changes are mostly contributed by the contraction of the Ir-Ir bond, which decreases from 3.27 to 3.22 Å. While EXAFS reflects average properties of the bulk material, we hypothesize that after 6 h CA, the Ir-Ir bond within the reconstructed surface phase shortens as Ca leaching occurs. While we cannot determine the exact structure of the surface reconstructed phase in isolation due to the interference from the bulk crystalline signal, we hypothesize that the reconstructed phase may have edgesharing [IrO<sub>6</sub>] octahedra. Considering edge-sharing octahedra have a much shorter Ir-Ir bond length of 3.14 Å (rutile IrO<sub>2</sub>), their generation is hypothesized to reduce the observed average bond length of Ir-Ir, albeit to a small extent, while the bulk remains pristine geometric structure with an Ir-Ir bond length of 3.27 Å.

## CONCLUSIONS

In summary, we have explored the degradation mechanism of  $Ca_2IrO_4$  for acidic OER. Similar to other iridium-based materials,  $Ca_2IrO_4$  displays an increase in intrinsic OER activity over initial electrochemical testing as well as an increase in capacitance.  $Ca_2IrO_4$  electrodes are stable over approximately 2 and 4 h at 1.60 and 1.576 V vs RHE, respectively, before degradation, during which the electrode requires increased overpotentials to reach 10  $mA/cm_{geo}^2$  exhibits nearly complete loss of capacitance, and experiences

reduced rates of Ir dissolution. The restructured surfaces formed under various controlled reaction conditions affect the stability of surface atoms and dissolved species, resulting in potential-dependent Ir transformation pathways. The prolonged OER performance by the catalysts in harsh oxidizing and acidic conditions causes an increase in average, bulk Ir oxidation state and a shortening of Ir-Ir bond lengths. A combination of materials characterization and EIS fitting supplies evidence that significant structural reorganization occurs within the surface layers, in conjunction with Ca and Ir dissolution, which likely comprises the majority of Ir-Ir bond length shortening. These changes eventually lead to the formation of a phase with more stable Ir sites but increasingly insulating behavior. Comparative studies on oxidized glassy carbon disk show that the catalyst degradation occurs on a faster timescale than carbon oxidation. However, future studies regarding long-term OER mechanism should take substrate oxidation into consideration since it could contribute to electrode instability. A fundamental understanding of the complex degradation reaction mechanism requires a combination of surface reconstruction, in situ metal dissolution, and robust, stable conductive supports for OER catalysts in acidic electrolyte under operating conditions.

### ASSOCIATED CONTENT

## **Solution** Supporting Information

The Supporting Information is available free of charge at https://pubs.acs.org/doi/10.1021/acs.energyfuels.3c01743.

Experimental details (materials synthesis, electrochemical testing, materials characterization); simulated diffraction pattern of Ca<sub>2</sub>IrO<sub>4</sub>; EIS fitting results; comparative study (evolution of impedance and geometric activity throughout stability testing) on pristine and preoxidized glassy carbon disk; comparative study (oxidation state and redox features of Au before and after OER, catalyst stability and Ir dissolution) on pristine gold disk; Ir XPS fitting results and additional Ca XPS spectra; XANES data and EXAFS data/fitting details; and references (PDF)

#### AUTHOR INFORMATION

## **Corresponding Author**

Linsey Seitz — Department of Chemical and Biological Engineering, Northwestern University, Evanston, Illinois 60208-3113, United States; ⊚ orcid.org/0000-0001-6831-6747; Email: linsey.seitz@northwestern.edu

#### Authors

Ruihan Li — Department of Chemical and Biological Engineering, Northwestern University, Evanston, Illinois 60208-3113, United States; orcid.org/0000-0001-5193-8523

Jane Edgington — Department of Chemical and Biological Engineering, Northwestern University, Evanston, Illinois 60208-3113, United States

Complete contact information is available at: https://pubs.acs.org/10.1021/acs.energyfuels.3c01743

## **Author Contributions**

R.L. contributed to the conceptualization, data curation, formal analysis, investigation, methodology, and writing of the original draft of this work. J.E. contributed to the data curation of *ex* 

situ XAS experiment, investigation, and review and editing of this work. L.S. contributed to the conceptualization, methodology, resources, supervision, and review and editing of this work. The manuscript was written through contributions of all authors. All authors have given approval to the final version of the manuscript.

### **Funding**

This material is based on work supported by a National Science Foundation CAREER Award (2144365-CBET).

#### Notes

The authors declare no competing financial interest.

#### ACKNOWLEDGMENTS

This work made use of the Jerome B. Cohen X-Ray Diffraction Facility supported by the MRSEC program of the National Science Foundation (DMR-1720139) at the Materials Research Center of Northwestern University and the Soft and Hybrid Nanotechnology Experimental (SHyNE) Resource (NSF ECCS-1542205). REACT acknowledged funding from Northwestern University Office of Research for purchase of the Micromeritics 3Flex instrument. This work made use of the EPIC and Keck-II facilities of Northwestern University's NUANCE Center, which has received support from the SHyNE Resource (NSF ECCS-2025633), the IIN, and Northwestern's MRSEC program (NSF DMR-1720139). Metal analysis was performed at the Northwestern University Quantitative Bioelement Imaging Center (QBIC) generously supported by the NIH under grant S10OD020118. MRCAT operations are supported by the Department of Energy and the MRCAT member institutions. This research used resources of the Advanced Photon Source, a U.S. Department of Energy (DOE) Office of Science User Facility, operated for the DOE office of Science by Argonne National Laboratory under contract no. DE-AC02-06CH11357. The authors graciously acknowledge the assistance of Rebecca Sponenburg with metal analysis at QBIC. The authors also graciously acknowledge the help of Joshua Wright, Mark Warren, Carlo Segre, Denis Keane, and Qing Ma for their assistance with XAS experimentation at the 10.ID Advanced Photon Source.

## ABBREVIATIONS

OER = oxygen evolution reaction

PEM = proton exchange membrane

RHE = reversible hydrogen electrode

EIS = electrochemical impedance spectroscopy

CV = cyclic voltammetry

CA = chronoamperometry

CP = chronopotentiometry

OCV = open circuit voltage

XRD = X-ray diffraction

HRTEM = high-resolution transmission electron microscopy

ICP-MS = inductively coupled plasma mass spectrometry

SEM = scanning electron microscopy

EDS = energy dispersive spectroscopy

XPS = X-ray photoelectron spectroscopy

XAS = X-ray absorption spectroscopy

XANES = X-ray absorption near edge spectroscopy

EXAFS = extended X-ray absorption fine structure.

Energy & Fuels pubs.acs.org/EF Article

#### REFERENCES

- (1) Wang, S.; Lu, A.; Zhong, C. J. Hydrogen production from water electrolysis: role of catalysts. *Nano Convergence* **2021**, *8*, 4.
- (2) Strickler, A. L.; Higgins, D.; Jaramillo, T. F. Crystalline Strontium Iridate Particle Catalysts for Enhanced Oxygen Evolution in Acid. ACS Appl. Energy Mater. 2019, 2, 5490–5498.
- (3) Song, C. W.; Lim, J.; Bae, H. B.; Chung, S.-Y. Discovery of crystal structure—stability correlation in iridates for oxygen evolution electrocatalysis in acid. *Energy Environ. Sci.* **2020**, *13*, 4178–4188.
- (4) Zhang, R.; Dubouis, N.; Ben Osman, M.; Yin, W.; Sougrati, M. T.; Corte, D. A. D.; Giaume, D.; Grimaud, A. A Dissolution/Precipitation Equilibrium on the Surface of Iridium-Based Perovskites Controls Their Activity as Oxygen Evolution Reaction Catalysts in Acidic Media. *Angew. Chem. Int. Ed.* **2019**, *58*, 4571–4575.
- (5) Li, N.; Cai, L.; Gao, G.; Lin, Y.; Wang, C.; Liu, H.; Liu, Y.; Duan, H.; Ji, Q.; Hu, W.; Tan, H.; Qi, Z.; Wang, L. W.; Yan, W. Operando Direct Observation of Stable Water-Oxidation Intermediates on Ca(2-x)IrO(4) Nanocrystals for Efficient Acidic Oxygen Evolution. *Nano Lett.* 2022, 22, 6988–6996.
- (6) Martelli, G. N.; Ornelas, R.; Faita, G. Deactivation Mechanisms of Oxygen Evolving Anodes at High Current Densities. *Electrochim. Acta* 1994, 39, 1551–1558.
- (7) Polonský, J.; Petrushina, I. M.; Christensen, E.; Bouzek, K.; Prag, C. B.; Andersen, J. E. T.; Bjerrum, N. J. Tantalum carbide as a novel support material for anode electrocatalysts in polymer electrolyte membrane water electrolysers. *Int. J. Hydrogen Energy* **2012**, *37*, 2173–2181.
- (8) Santos, D.; Lopes, A.; Pacheco, M. J.; Gomes, A.; Ciríaco, L. The Oxygen Evolution Reaction at Sn-Sb Oxide Anodes: Influence of the Oxide Preparation Mode. *J. Electrochem. Soc.* **2014**, *161*, H564—H572.
- (9) Friebel, D.; Louie, M. W.; Bajdich, M.; Sanwald, K. E.; Cai, Y.; Wise, A. M.; Cheng, M.-J.; Sokaras, D.; Weng, T.-C.; Alonso-Mori, R.; Davis, R. C.; Bargar, J. R.; Nørskov, J. K.; Nilsson, A.; Bell, A. T. Identification of Highly Active Fe Sites in (Ni,Fe)OOH for Electrocatalytic Water Splitting. *J. Am. Chem. Soc.* **2015**, 137, 1305–1313.
- (10) Kasian, O.; Grote, J. P.; Geiger, S.; Cherevko, S.; Mayrhofer, K. J. J. The Common Intermediates of Oxygen Evolution and Dissolution Reactions during Water Electrolysis on Iridium. *Angew. Chem. Int. Ed. Engl.* **2018**, *57*, 2488–2491.
- (11) Binninger, T.; Mohamed, R.; Waltar, K.; Fabbri, E.; Levecque, P.; Kötz, R.; Schmidt, T. J. Thermodynamic explanation of the universal correlation between oxygen evolution activity and corrosion of oxide catalysts. *Sci. Rep.* **2015**, *5*, 12167.
- (12) Kuo, D.-Y.; Kawasaki, J. K.; Nelson, J. N.; Kloppenburg, J.; Hautier, G.; Shen, K. M.; Schlom, D. G.; Suntivich, J. Influence of Surface Adsorption on the Oxygen Evolution Reaction on IrO2(110). *J. Am. Chem. Soc.* **2017**, *139*, 3473–3479.
- (13) Rafiee, M.; Mayer, M. N.; Punchihewa, B. T.; Mumau, M. R. Constant Potential and Constant Current Electrolysis: An Introduction and Comparison of Different Techniques for Organic Electrosynthesis. J. Org. Chem. 2021, 86, 15866–15874.
- (14) McCrory, C. C. L.; Jung, S.; Ferrer, I. M.; Chatman, S. M.; Peters, J. C.; Jaramillo, T. F. Benchmarking hydrogen evolving reaction and oxygen evolving reaction electrocatalysts for solar water splitting devices. *J. Am. Chem. Soc.* **2015**, *137*, 4347–4357.
- (15) McCrory, C. C. L.; Jung, S.; Peters, J. C.; Jaramillo, T. F. Benchmarking heterogeneous electrocatalysts for the oxygen evolution reaction. *J. Am. Chem. Soc.* **2013**, *135*, 16977–16987.
- (16) Li, G.; Anderson, L.; Chen, Y.; Pan, M.; Abel Chuang, P.-Y. New insights into evaluating catalyst activity and stability for oxygen evolution reactions in alkaline media. *Sustainable Energy Fuels* **2018**, *2*, 237–251.
- (17) Yang, L.; Yu, G.; Ai, X.; Yan, W.; Duan, H.; Chen, W.; Li, X.; Wang, T.; Zhang, C.; Huang, X.; Chen, J. S.; Zou, X. Efficient oxygen evolution electrocatalysis in acid by a perovskite with face-sharing IrO(6) octahedral dimers. *Nat. Commun.* **2018**, *9*, 5236.
- (18) Fabbri, E.; Nachtegaal, M.; Binninger, T.; Cheng, X.; Kim, B.-J.; Durst, J.; Bozza, F.; Graule, T.; Schäublin, R.; Wiles, L.; Pertoso, M.;

- Danilovic, N.; Ayers, K. E.; Schmidt, T. J. Dynamic surface self-reconstruction is the key of highly active perovskite nano-electrocatalysts for water splitting. *Nat. Mater.* **2017**, *16*, 925–931.
- (19) Chen, G.; Zhou, W.; Guan, D.; Sunarso, J.; Zhu, Y.; Hu, X.; Zhang, W.; Shao, Z. Two orders of magnitude enhancement in oxygen evolution reactivity on amorphous  $Ba_{0.5}Sr_{0.5}Co_{0.8}Fe_{0.2}O_{3-\delta}$  nanofilms with tunable oxidation state. *Sci. Adv.* **2017**, 3, No. e1603206.
- (20) Song, C. W.; Suh, H.; Bak, J.; Bae, H. B.; Chung, S.-Y. Dissolution-Induced Surface Roughening and Oxygen Evolution Electrocatalysis of Alkaline-Earth Iridates in Acid. *Chem* **2019**, *S*, 3243–3259.
- (21) Diaz-Morales, O.; Raaijman, S.; Kortlever, R.; Kooyman, P. J.; Wezendonk, T.; Gascon, J.; Fu, W. T.; Koper, M. T. M. Iridium-based double perovskites for efficient water oxidation in acid media. *Nat. Commun.* **2016**, *7*, 12363.
- (22) Sarkozy, R. F.; Moeller, C. W.; Chamberland, B. L. The Characterization of Calcium Iridium Oxides. *J. Solid State Chem.* **1974**, *9*, 242–246.
- (23) Grimaud, A.; Demortière, A.; Saubanère, M.; Dachraoui, W.; Duchamp, M.; Doublet, M.-L.; Tarascon, J.-M. Activation of surface oxygen sites on an iridium-based model catalyst for the oxygen evolution reaction. *Nat. Energy* **2017**, *2*, 16189.
- (24) Jung, S.; McCrory, C. C. L.; Ferrer, I. M.; Peters, J. C.; Jaramillo, T. F. Benchmarking nanoparticulate metal oxide electrocatalysts for the alkaline water oxidation reaction. *J. Mater. Chem. A* **2016**, *4*, 3068–3076.
- (25) Wei, C.; Sun, S.; Mandler, D.; Wang, X.; Qiao, S. Z.; Xu, Z. J. Approaches for measuring the surface areas of metal oxide electrocatalysts for determining their intrinsic electrocatalytic activity. *Chem. Soc. Rev.* **2019**, *48*, 2518–2534.
- (26) Edgington, J.; Deberghes, A.; Seitz, L. C. Glassy Carbon Substrate Oxidation Effects on Electrode Stability for Oxygen Evolution Reaction Catalysis Stability Benchmarking. *ACS Appl. Energy Mater.* **2022**, *5*, 12206–12218.
- (27) Orazem, M. E.; Tribollet, B. Methods for Representing Impedance. *Electrochem. Impedance Spectrosc.* **2008**, 307–331.
- (28) Orazem, M. E.; Pébère, N.; Tribollet, B. Enhanced graphical representation of electrochemical impedance data. *J. Electrochem. Soc.* **2006**, *153*, B129–B136.
- (29) Huang, V. M.-W.; Vivier, V.; Orazem, M. E.; Pébère, N.; Tribollet, B. The apparent constant-phase-element behavior of an ideally polarized blocking electrode. A global and local impedance analysis. *J. Electrochem. Soc.* 2007, 154, S6–S6.
- (30) Lyovich, V. F. Equivalent-Circuit Elements and Modeling of the Impedance Phenomenon. *Impedance Spectrosc.* **2012**, 37–47.
- (31) Yi, Y.; Weinberg, G.; Prenzel, M.; Greiner, M.; Heumann, S.; Becker, S.; Schlögl, R. Electrochemical corrosion of a glassy carbon electrode. *Catal. Today* **2017**, *295*, 32–40.
- (32) Dickens, C. F.; Nørskov, J. K. A Theoretical Investigation into the Role of Surface Defects for Oxygen Evolution on RuO2. *J. Phys. Chem. C* **2017**, *121*, 18516–18524.
- (33) Geiger, S.; Kasian, O.; Ledendecker, M.; Pizzutilo, E.; Mingers, A. M.; Fu, W. T.; Diaz-Morales, O.; Li, Z.; Oellers, T.; Fruchter, L.; Ludwig, A.; Mayrhofer, K. J. J.; Koper, M. T. M.; Cherevko, S. The stability number as a metric for electrocatalyst stability benchmarking. *Nat. Catal.* **2018**, *1*, 508–515.
- (34) Edgington, J.; Seitz, L. C. Advancing the Rigor and Reproducibility of Electrocatalyst Stability Benchmarking and Intrinsic Material Degradation Analysis for Water Oxidation. *ACS Catal.* **2023**, 3379–3394.
- (35) Hubert, M. A.; Gallo, A.; Liu, Y.; Valle, E.; Sanchez, J.; Sokaras, D.; Sinclair, R.; King, L. A.; Jaramillo, T. F. Characterization of a Dynamic Y<sub>2</sub>Ir<sub>2</sub>O<sub>7</sub> Catalyst during the Oxygen Evolution Reaction in Acid. *J. Phys. Chem. C* **2022**, *126*, 1751–1760.
- (36) Zhang, X.; Su, H.; Sun, X.; Yang, C.; Li, Y.; Zhang, H.; Zhou, W.; Liu, M.; Cheng, W.; Wang, C.; Wang, H.; Liu, Q. Quick evolution of edge-shared metal-oxygen octahedrons for boosting acidic water oxidation. *Nano Energy* **2022**, *102*, No. 107680.